WILEY-VCH

FULL PAPER

A combined "electrochemical-frustrated Lewis pair" approach to hydrogen activation: surface catalytic effects at platinum electrodes

Elliot J. Lawrence,[a] Robin J. Blagg,[a] David L. Hughes,[a] Andrew E. Ashley,[b] Gregory G. Wildgoose[a]*

Abstract: In this report, we extend our "combined electrochemical-frustrated Lewis pair" approach to include Pt electrode surfaces for the first time. We find that the voltammetric response of an electrochemical-frustrated Lewis pair system involving the $B(C_6F_5)_3$ / $[B(C_6F_5)_3H]^-$ redox couple exhibits a strong surface electrocatalytic effect at Pt electrodes. Using a combination of kinetic competition studies in the presence of a H-atom scavenger, 6-bromohexene, and by changing the steric bulk of the Lewis acid borane catalyst from $B(C_6F_5)_3$ to $B(C_6Cl_5)_3$, the mechanism of electrochemical-FLP reactions on Pt surfaces is shown to be dominated by hydrogen atom transfer (HAT) between Pt, [Pt–H] adatoms, and transient $[HB(C_6F_5)_3]^•$ electrooxidation intermediates. These findings provide further insight into this new area of combining electrochemical and FLP reactions, and proffers additional avenues for exploration beyond energy generation, such as in electrosynthesis.

Introduction

The field of frustrated Lewis pair (FLP) chemistry has continued to grow rapidly since the pioneering work of Stephan's group in 2006.[1] The combination of suitably sterically encumbered Lewis acid and Lewis base (LB) components (that are incapable of forming classical Lewis adducts) were found to heterolytically cleave H_2, resulting in hydridic and protic components. Whilst the inception of FLPs is relatively recent, Brown and co-workers first uncovered the concept of steric frustration in 1942, when they failed to form a Lewis adduct from the combination of lutidine and BMe_3.[2] The application of FLPs for the activation of H_2 and other small molecules has been reviewed extensively.[3–6] For main group FLPs, the Lewis acid component is typically based on electron-deficient boranes, typically $B(C_6F_5)_3$ and its derivatives,[1,7–10] although FLP H_2 activation has also been achieved using analogous $Al(C_6F_5)_3$[11] and boranes that do not contain C_6F_5 groups.[12–17] FLPs are not limited to the main group;[18–20] Wass and co-workers previously demonstrated the ability of zirconocene-phosphinoaryloxide complexes to mimic the reactivity of FLPs and offer additional, unprecendented reactivity towards small molecules.[19]

The majority of literature reports focus on delivering the resulting hydride to reduce a wide range of functional groups including imines, enamines and nitriles;[21–23] aldehydes;[8] and activate small molecules such as CO_2.[24–26]

We have recently introduced a new approach to H_2 oxidation by combining FLP chemistry to heterolytically cleave H_2 with *in situ* electrochemical oxidation of the resultant borohydride.[27,28] Through combining Stephan's archetypal $B(C_6F_5)_3$ (**1**)/*t*Bu_3P FLP with the electrochemical oxidation of the generated $[HB(C_6F_5)_3]^-$, [**1**–H]$^-$, the voltage required for H_2 oxidation at a glassy carbon electrode (GCE) was found to be reduced by 610 mV (equivalent to a reduction in the required energetic driving force of 177.7 kJ mol^{-1}). The digital simulation of voltammetric data combined with chemical mechanistic studies and DFT calculations allowed us to propose that the oxidation of [**1**–H]$^-$ follows the mechanism at carbon electrode surfaces as shown in Scheme 1.

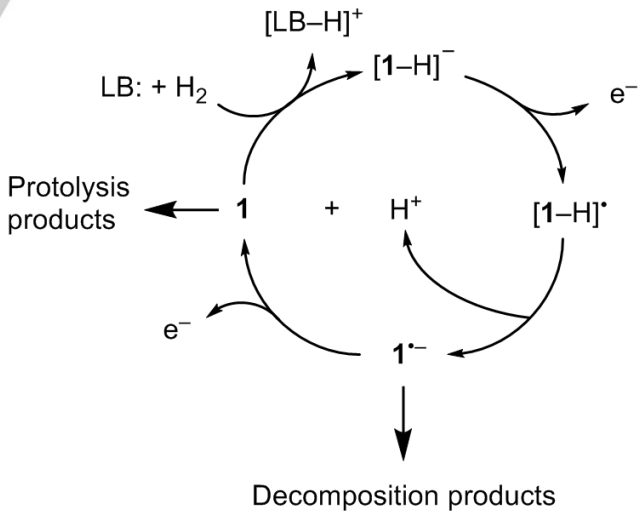

Scheme 1. The proposed redox mechanism for the oxidation of [**1**–H]$^-$ at a glassy carbon electrode surface (LB = Lewis base).[27]

[a] Mr E.J. Lawrence, Dr R.J. Blagg, Dr D.L. Hughes, Dr G.G.Wildgoose*
Energy Materials Laboratory
School of Chemistry
University of East Anglia
Norwich Research Park
Norwich, NR4 7TJ,
United Kingdom
E-mail: g.wildgoose@uea.ac.uk

[b] Dr A.E. Ashley
Department of Chemistry
Imperial College London
South Kensington,
London, SW7 2AZ
United Kingdom
E-mail: a.ashley@imperial.ac.uk

Supporting information for this article is given via a link at the end of the document.

This concept holds great promise for precious metal-free energy generation applications such as fuel cell technologies, where extensive research efforts into aqueous-phase borohydride, $[BH_4]^-$ electrooxidation at Pt electrodes have already been invested.[29–33] Aside from our recent studies using carbon electrodes, the non-aqueous redox chemistry of bulkier borohydrides such as [**1**–H]$^-$,[27,34] and their parent electron-deficient, Lewis acidic boranes,[35,36] remain largely unexplored. Therefore, in order to better understand the oxidation mechanism of important intermediates such as [**1**–H]$^-$ in combined electrochemical-FLP systems, in this report we seek to explore and understand the electrochemical behaviour of [**1**–H]$^-$ at Pt electrode surfaces.

Results and Discussion

The oxidative redox chemistry of an authentic sample of [*n*Bu$_4$N][**1**–H] at 2.3 mM and 4.8 mM concentrations in CH_2Cl_2 solutions containing 0.05 M [*n*Bu$_4$N][B(C$_6$F$_5$)$_4$] as a weakly coordinating electrolyte,[36] was explored at a Pt macrodisk electrode using cyclic voltammetry (Figure 1). As the potential was swept in a positive direction, a large, well-defined oxidative wave was observed at +0.49 V *vs* $Cp_2Fe^{0/+}$. The potential scan direction was reversed just before the limit of the solvent potential window, whereupon the current was observed to cross-over the forward-going current, and remained positive (indicating an oxidation was occurring) at potentials more negative than the oxidation potential of [**1**–H]$^-$. The current then gradually decreased (whilst still remaining positive) until it re-crossed the forward scan in the region of −0.30 to −0.25 V *vs* $Cp_2Fe^{0/+}$; a series of small, ill-defined reduction waves were observed at more negative potentials.

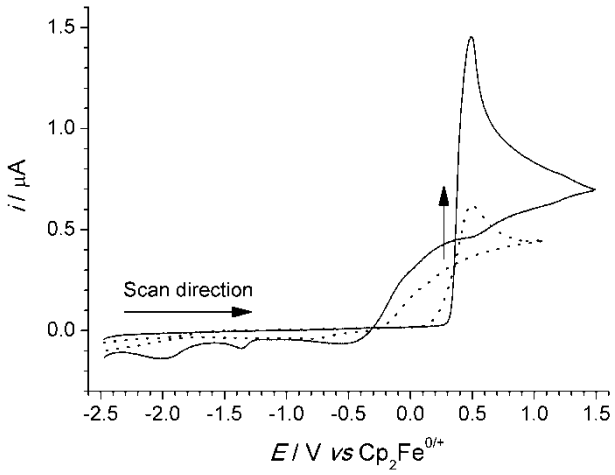

Figure 1. Cyclic voltammetry of [*n*Bu$_4$N][**1**–H] at a Pt macrodisk electrode (2.3 mM (dashed line) and 4.8 mM (solid line); 0.05 M [*n*Bu$_4$N][B(C$_6$F$_5$)$_4$], CH_2Cl_2) recorded at a scan rate of 100 mV s^{-1}.

The observed voltammetric response at a Pt macrodisk electrode is in stark contrast to what has been observed previously at a GCE (Figure 2), where a more typical electrochemically reversible, but chemically irreversible oxidation wave is observed with no observable corresponding reduction wave, no current-crossing, and a small reduction wave at a more negative potential assigned to the reduction of the parent B(C$_6$F$_5$)$_3$, **1**.[27,36] The observation of a crossing-current in cyclic voltammetry is unusual; for an oxidation process, this signifies the formation of a new electroactive product that has a much lower reduction potential. This effect is only observed in either special cases of a homogenous ECE-type mechanism,[37] or when a change in the electrode surface structure occurs, usually during an electrocatalytic process e.g. significant current-crossover is observed when methanol is oxidized at Pt electrodes, owing to the formation of various adsorbed intermediate species that are electroactive at lower oxidation potentials.[38] In our case, the height at which the reverse current crosses the forward-going current strongly suggests that the latter scenario, a surface change on the electrode, is likely responsible for this effect.

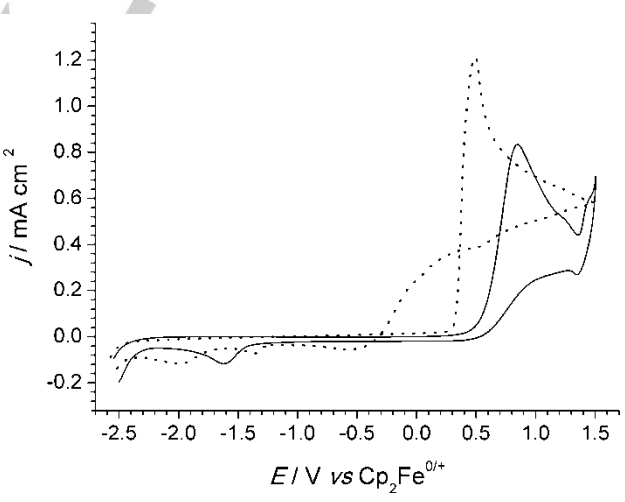

Figure 2. Comparison of the voltammetry for a 5 mM solution of [*n*Bu$_4$N][**1**–H] recorded at Pt (dashed line) and glassy carbon (solid line) macrodisk electrodes in CH_2Cl_2, containing 0.05 M [*n*Bu$_4$N][B(C$_6$F$_5$)$_4$] electrolyte, at a scan rate of 100 mV s^{-1}. Note that the current density, *j*, is plotted to allow a direct comparison between electrodes of different geometric areas.

It is clear from these results that the Pt electrode is non-innocent and exhibits strong electrocatalytic properties. For example, the rate of electron transfer during the oxidation of [**1**–H]$^-$ is very much faster at the Pt electrode than at the GCE, leading to a much steeper gradient in the rising part of the oxidation wave, a sharper peak, and an overall larger peak current density recorded at the Pt electrode (Figure 2). Furthermore, the oxidative peak current is shifted by –390 mV at Pt compared to the GCE – evidence of strong surface electrocatalysis.

In order to explain these phenomena, we propose a modification to our earlier mechanism for the oxidation of [**1**–H]$^-$ on a GCE,[27] that takes into account the well-documented ability

of Pt surfaces to adsorb H atoms, as is observed in the direct, electrocatalytic oxidation of H_2 at Pt electrodes in aqueous electrolytes (Scheme 2).[39,40] The initial step, the one-electron oxidation of [**1**–H]$^-$, occurs at both Pt and GCE to form a transient [$HB(C_6F_5)_3$]$^\bullet$ radical, [**1**–H]$^\bullet$. DFT calculations show that the SOMO of [**1**–H]$^\bullet$ is somewhat delocalised over the aryl rings, however, the majority of spin-density is located in the B–H bond which is significantly weakened, with a bond enthalpy of *ca*. 30 kJmol^{-1}.[27] At carbon electrodes, this radical dissociates very rapidly to form a proton and a **1**$^{\bullet-}$ radical anion which undergoes further oxidation in competition with its decomposition in solution (Scheme 1). However, the Pt electrode surface is able to compete effectively with the dissociation step and abstracts a hydrogen atom from [**1**–H]$^\bullet$, liberating the parent borane, **1**, and forming a H adatom on the surface of the electrode, Pt–H. This hydrogen atom transfer (HAT) reaction effects a change on the surface of the electrode. As the oxidation potential of Pt–H is very much less than the potential at this point in the cyclic voltammogram (close to the oxidation peak potential observed) it rapidly undergoes a second one-electron oxidation to form a proton and regenerate the Pt active site on the electrode in an electrocatalytic fashion. This process is occurring throughout the beginning of the reverse sweep, such that there is a significant surface concentration of Pt–H at the potential where the current crosses-over the forward-going scan, and this continues to be oxidized, giving rise to an oxidative current at potentials more negative than that of the oxidation of [**1**–H]$^-$, until the potential approaches the reduction potential of the Pt–H system around −0.3 V vs $Cp_2Fe^{0/+}$, whereupon the current decreases, and the reverse reaction, reduction of protons to form Pt–H, occurs at the electrode surface.

$$[HB(C_6F_5)_3]^- \rightleftharpoons [HB(C_6F_5)_3]^\bullet + e^- \quad E_1 \text{ step}$$

$$[HB(C_6F_5)_3]^\bullet + Pt_{surface} \xrightarrow{k_{f1}} B(C_6F_5)_3 + [Pt\text{–}H]_{surface} \quad C_1 \text{ step}$$

$$[Pt\text{–}H]_{surface} \rightleftharpoons Pt_{surface} + H^+ + e^- \quad E_2 \text{ step}$$

$$[Pt\text{–}H]_{surface} + Sub \xrightarrow{k_{f2}} Pt_{surface} + [Sub\text{–}H]^\bullet \quad C_2 \text{ step}$$

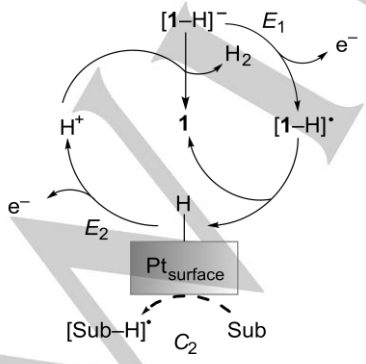

Scheme 2. The proposed redox mechanism with individual steps for the electrocatalytic oxidation of [**1**–H]$^-$ at a Pt electrode surface, (labelled in Testa-Reinmuth notation, top) and the schematic representation of the entire mechanistic cycle (bottom). The decomposition pathways of **1** and **1**$^{\bullet-}$ are omitted for clarity (see **Scheme 1** and text for details). Also shown is the competing hydrogen atom transfer reaction, labelled as C_2, between a substrate, Sub, and the $[Pt\text{–}H]_{surface}$ species.

Note that all electron transfer steps are reversible, and therefore subject to Nernstian equilibria.[37] Perturbation of the surface concentration of [**1**–H]$^\bullet$ by competition with Pt–H formation is responsible for the reduction in the apparent oxidation potential of [**1**–H]$^-$ at Pt vs GCE, and explains why the onset of oxidation occurs on Pt at less positive potentials than at glassy carbon, *i.e.* is electrocatalytic at Pt. With reference to our earlier work,[27,36] we assign the small reduction wave at *ca.* −2.0 V *vs* $Cp_2Fe^{0/+}$ to the reduction of **1**. Note we have shown that this arises mainly by the reaction of incoming [**1**–H]$^-$ reacting with electrogenerated protons, hence why the reduction peak is small in comparison to the oxidation peak; most of the electrogenerated **1** undergoes protolytic decomposition.[27] Proton reduction on the polycrystalline Pt surface in CH_2Cl_2 may also be responsible for the small, ill-defined reduction waves seen between *ca.* –0.3 and –2.0 V, an assignment supported by the observation of similar voltammetric features when CH_2Cl_2 is spiked with the oxonium acid, $[H(OEt_2)_2][B(C_6F_5)_4]$.[41]

The change on the surface of the electrode unfortunately prevents us from attempting digital simulation of the voltammetric data, to extract the relevant kinetic and thermodynamic parameters and to confirm the proposed mechanism by fitting the experimental data. Nonetheless, evidence to support our proposed mechanism was obtained by: 1) competition experiments with an hydrogen atom scavenger; 2) increasing the steric bulk surrounding the B–H bond by replacing C_6F_5 groups with C_6Cl_5 groups as $[HB(C_6Cl_5)_3]^-$, [**2**–H]$^-$.

In order to investigate our proposed mechanism we conducted cyclic voltammetry of [**1**–H]$^-$ in the presence of increasing molar equivalents of 6-bromo-1-hexene. This well-known radical clock acts as a scavenger for H atoms, forming 5-hexenyl radical intermediates that cyclize at a known rate[42–48] and was chosen as neither the parent radical clock nor any of the intermediate radicals or cyclized products have any redox chemistry in the potential window of interest. Figure 3 shows the cyclic voltammograms recorded for the oxidation of [**1**–H]$^-$ in the presence of 0-10 molar equivalents of the radical clock.

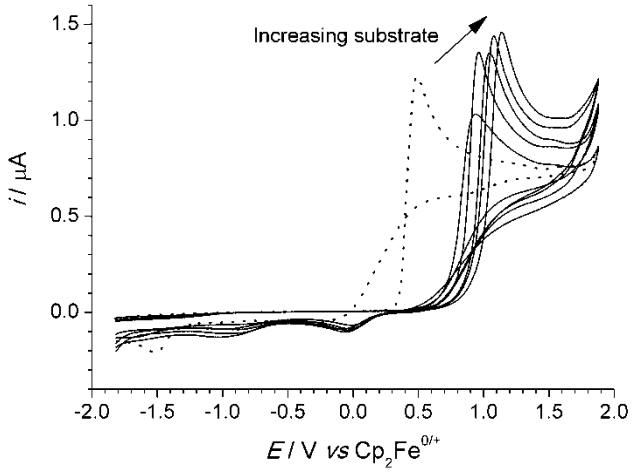

Figure 3. Overlaid cyclic voltammograms of a 4.8 mM solution of [*n*Bu$_4$N][**1**–H] (dotted line) with increasing addition of 6-bromo-1-hexene (black lines; from left to right: 1, 2, 4, 8 and 10 molar equivalents) recorded at a Pt macrodisk electrode in CH_2Cl_2 containing 0.05 M [*n*Bu$_4$N][B(C_6F_5)$_4$] electrolyte at a voltage scan rate of 100 mV s^{-1}.

Upon the addition of a first molar equivalent of radical clock, the oxidation wave of [**1**–H]$^-$ shifts to more positive potentials, decreases in height, and crucially, does not exhibit any current cross-over effects. Indeed the voltammetry is very similar to that observed at a bare GCE both in terms of peak potential, wave-shape and peak current. This can be understood in terms of the radical clock competing very effectively with the Pt electrode surface to abstract a hydrogen atom from the transient [**1**–H]$^•$ species, thus preventing the formation of Pt–H on the surface. Thus, the catalytic oxidation step for the Pt–H surface species at reduced potentials (Scheme 2) is "switched-off" and the oxidation mechanism of [**1**–H]$^-$ now occurs along the same reaction pathway as it does at the GCE electrode (Scheme 1). Thus the H atom scavenger 6-bromo-1-hexene acts as a competitive inhibitor for any surface electrocatalytic step by the Pt electrode. As the concentration of radical clock is increased the peak potential gradually increases as does the peak current. The increase in peak potential is a direct effect of the reaction between 6-bromo-1-hexene and [**1**–H]$^•$ which perturbs the Nernstian equilibrium governing the initial oxidation of [**1**–H]$^-$ thereby increasing the peak potential. The increase in peak current can be understood in similar terms: the abstraction of a H atom from [**1**–H]$^•$ prevents its dissociation into protons, and therefore inhibits the reaction of protons with a second incoming [**1**–H]$^-$ (see Scheme 1) which would otherwise lead to a decrease in the observed oxidation current.

Another synthetic route to inhibit the formation of Pt–H surface adatom formation is to increase the steric bulk around the B–H bond, and thus sterically "shield" the hydrogen atom from any interaction with the Pt electrode surface. Our approach required the synthesis of the hitherto unknown borohydride, [*n*Bu$_4$N][HB(C_6Cl_5)$_3$], [*n*Bu$_4$N][**2**–H], by treating the parent perchlorinated analogue of **1**, B(C_6Cl_5)$_3$ (**2**), with Na[HBEt$_3$] in toluene at 80 °C, and then metathesizing the resulting Na$^+$ cation with [*n*Bu$_4$N]$^+$ to impart the required solubility for non-aqueous electrochemistry. Note that this Lewis acidic borane was chosen because we have previously reported the synthesis and voltammetric characterization of **2**,[35] which is a much more electron deficient borane than **1** (despite Cl being less electronegative than F, the Hammet parameter at the para ring position of Cl is greater (σ_{para}(Cl) = 0.227; σ_{para}(F) = 0.062) as a result of weaker (*3p–2p*) π-overlap with the aromatic ring), and that the -C_6Cl_5 substituents have a greater steric profile than -C_6F_5 (see Figure 4 for crystal structure of [*n*Bu$_4$N][**2**–H] and space filling model).

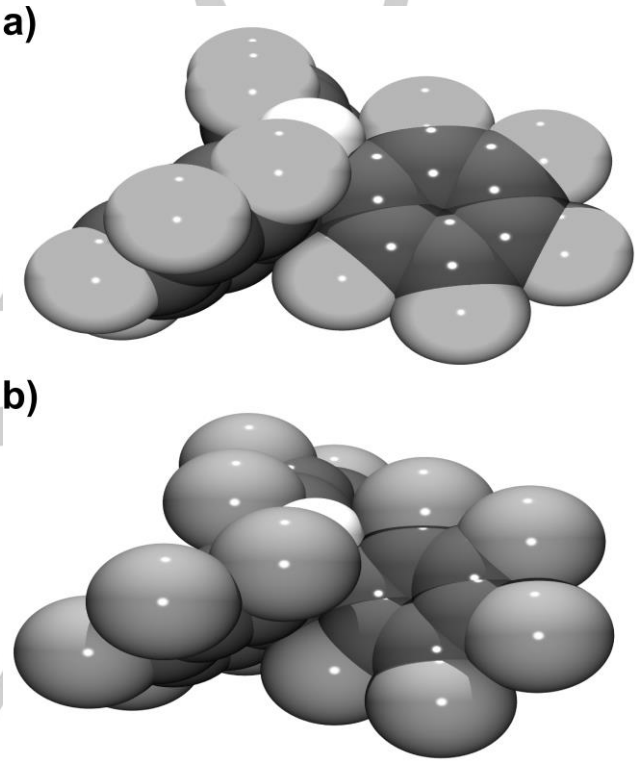

Figure 4. Space-filling view of the ions of a) [**1**–H]$^-$ and b) [**2**–H]$^-$, showing the extent of steric shielding of the B–H bond by the surrounding C_6Cl_5 groups. Only the major components of disordered groups are shown.

Cyclic voltammetry of [**2**–H]$^-$ (Figure 5) indicates that it is oxidized at a slightly higher potential (ca. 100 mV) than [**1**–H]$^-$, suggesting that [**2**–H]$^-$ is less hydridic than [**1**–H]$^-$. This is consistent with the parent borane, **2**, being more electrophilic than **1**.[35] In the case of [**2**–H]$^-$, however, no current cross-over is observed at any scan rate, indicating that the steric bulk around the B–H bond in [**2**–H]$^-$ is sufficient to prevent the formation of any Pt–H surface species, and thus any electrocatalysis by the electrode surface, and lends further support for our proposed mechanism for the electrocatalytic oxidation of [**1**–H]$^-$ in Scheme 2. Instead a new, quasi-reversible redox wave is observed at a mid-peak potential of +0.98 mV *vs* $Cp_2Fe^{0/+}$. Noting that the height of the first oxidation wave corresponds to a single-electron oxidation, and that in the parent Lewis acid, **2**, the central boron

atom is sufficiently sterically shielded that its radical anion, formed upon electroreduction, is stable in solution (unlike that of **1**), we tentatively propose that this voltammetric feature corresponds to the one-electron oxidation of [**2**–H]$^{\bullet}$ radicals, which are relatively long-lived intermediates in contrast to [**1**–H]$^{\bullet}$, and which occurs alongside competing solvolysis/dissociation steps. Whether this is indeed due to an identifiable B–H bonded species or whether free H$^{\bullet}$ is dissociatively formed in a "cage" within the void formed by the central B-atom and neighboring aryl-Cl groups, and possibly the solvent, is the subject of ongoing investigations. What is clear is that this new voltammetric feature only arises as a result of the increased steric bulk surrounding the central boron atom.

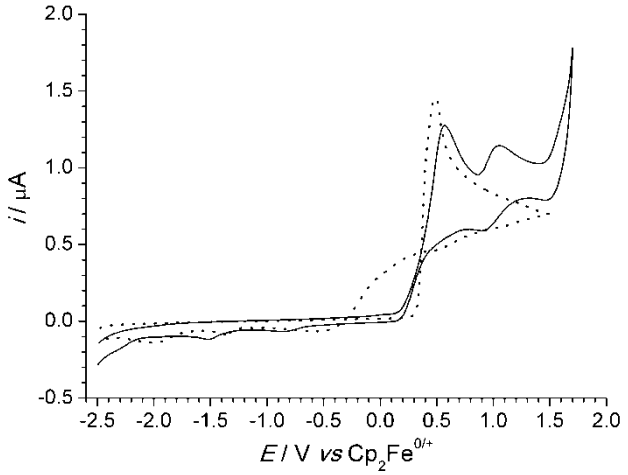

Figure 5. Overlaid cyclic voltammetry comparing the oxidation of 5.0 mM solutions of [**1**–H]$^{-}$ (dashed line) and [**2**–H]$^{-}$ (solid line) at a Pt macrodisk electrode (0.05 M [*n*Bu$_4$N][B(C$_6$F$_5$)$_4$], CH$_2$Cl$_2$, scan rate 100 mV s^{-1}).

Finally, for completeness, we examined the *in situ* combined electrochemical frustrated Lewis pair activation of H_2 at Pt, in much the same fashion as our previous efforts at a GCE. Figure 6 shows the voltammetry of a 1:1 solution of the FLP B(C$_6$F$_5$)$_3$/TMP (TMP = 2,2,6,6-tetramethylpiperidine, a frustrated Lewis base) at Pt whereupon the reduction of **1** and the oxidation of TMP are initially clearly observed under N_2 (dotted line, Figure 6). H_2 was bubbled through the electrolyte solution for a period of 1 hour before a second cyclic voltammogram was recorded (solid line, Figure 6). Although the kinetics of H_2 cleavage by this FLP system are relatively slow, even after 1 hour of sparging with H_2, clear voltammetric evidence for the formation of [**1**–H]$^{-}$ is observed as a new peak at +0.43 mV *vs* Ag$^{0/+}$, intermediate between the oxidation of TMP and the reduction of **1**. Although this new peak is broadened compared with an authentic sample of [**1**–H]$^{-}$ due to its low concentration, it is characteristic of the voltammetry of [**1**–H]$^{-}$, and evidence for the *in situ* combined electrochemical frustrated Lewis pair activation of H_2. Whilst this result is less applicable to energy applications, where one would directly oxidize H_2 in aqueous electrolyte at Pt, in light of our findings above, it does open up the tantalizing prospect of using combined electrochemical frustrated Lewis pair chemistry to electrocatalytically activate H_2 for HAT reactions with potential applications in novel electrosynthesis. This prospect forms part of our ongoing collaborative research efforts to further develop our combined electrochemical-frustrated Lewis pair approach.

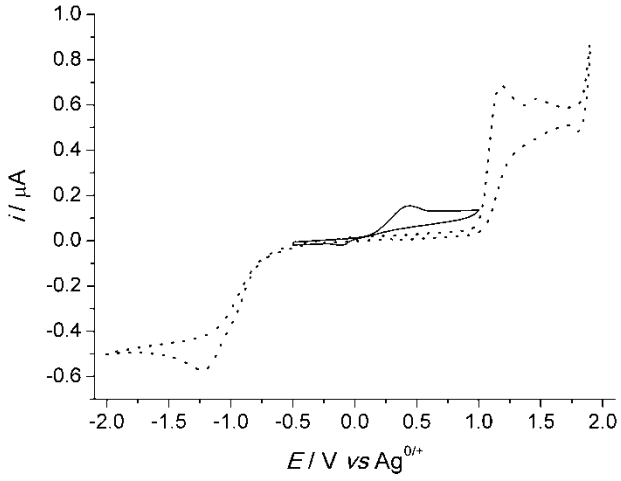

Figure 6. Overlaid cyclic voltammograms demonstrating the TMP/B(C$_6$F$_5$)$_3$ FLP system (5 mM equimolar solutions) before (dotted line) and after (solid line) a 1 h sparge with H_2 (0.05 M [*n*Bu$_4$N][B(C$_6$F$_5$)$_4$], CH$_2$Cl$_2$ electrolyte, scan rate 100 mV s^{-1}).

Conclusions

We have investigated the hitherto unexplored electrochemistry of bulky borohydrides, namely the tris(pentafluorophenyl)borohydride anion and its perchlorinated analogue, at Pt electrode surfaces. We have found the Pt electrode exhibits strong electrocatalytic properties within the electrochemical-FLP system. Evidence of strong surface-based electrocatalysis was given by a significant current-crossover (surface change) in the cyclic voltammetry of authentic [**1**–H]$^{-}$ and, more importantly, a 390 mV reduction in the oxidation peak potential compared to GCE materials. The electrocatalytic effect of Pt, which involves HAT reactions, was "switched off" in the presence of a competing radical scavenger. In addition, this electrocatalysis was not observed when [**1**–H]$^{-}$ was substituted for a relatively bulky perchlorinated analogue, [**2**–H]$^{-}$. The use of platinum electrodes in conjunction with combined electrochemical-FLP systems permit a significant energy saving for the effective conversion of chemical energy, stored in the H–H bond, to electrical energy that is available for work. The elucidated electrochemical mechanism suggests the prospect of using combined electrochemical frustrated Lewis pair chemistry to activate H_2 for HAT reactions. This opens up a completely new area for exploration for the combined electrochemical–frustrated Lewis pair concept, with potential applications in electrosynthetic catalysis.

Experimental Section

General. All synthetic reactions and manipulations were performed under a dry N_2 atmosphere (BOC Gases) using standard Schlenk-line techniques on a dual manifold vacuum/inert gas line or either a Saffron or MBraun glovebox. All glassware was flame-dried under vacuum before use. Anhydrous solvents were dried via distillation over appropriate drying agents: molten Na for toluene; CaH_2 for dichloromethane. All solvents were sparged with nitrogen gas to remove any trace of dissolved oxygen and stored in ampules over activated 4 Å molecular sieves. Na[$HBEt_3$] (1.0 M in toluene) was purchased from Sigma-Aldrich and used without further purification. *n*Bu_4NCl was purchased from Alfa Aesar and recrystallized from anhydrous acetone prior to use. Hydrogen gas (99.995 %) was purchased from BOC gases and passed over drying columns containing P_4O_{10} and 4 Å molecular sieves prior to use. Deuterated NMR solvents ([D_6]DMSO, 99.9 %; $CDCl_3$, 99.8 %) were purchased from Cambridge Isotope Laboratories Inc. and were dried over P_4O_{10}, degassed using a triple freeze-pump-thaw cycle and stored over activated 4 Å molecular sieves. [*n*Bu_4N][**1**–H],[27] **1**,[49] **2**,[35] [*n*Bu_4N][$B(C_6F_5)_4$][50] and *t*Bu_3P[51] were prepared according to literature methods. NMR spectra were recorded using either a Bruker Avance DPX-300 or DPX-500 MHz spectrometer. Chemical shifts are reported in ppm and are referenced relative to appropriate standards; ^{11}B is relative to $Et_2O{\cdot}BF_3$, ^{31}P is relative to 85 % H_3PO_4.

Electrochemistry. All electrochemical experiments were performed using either an Autolab PGSTAT 30 or PGSTAT 302N computer-controlled potentiostat (Utrecht, The Netherlands). Cyclic voltammetry (CV) was performed using a three-electrode configuration consisting of either a glassy carbon macrodisk working electrode (GCE) (diameter of 3 mm; BASi, Indiana, USA) or a Pt macrodisk working electrode (diameter of 0.4 mm, 99.99 %; GoodFellow, Cambridge, UK), combined with a Pt wire counter electrode (99.99 %; GoodFellow, Cambridge, UK) and a Ag wire pseudoreference electrode (99.99 %; GoodFellow, Cambridge, UK). The GCE was polished between experiments using successive grades of diamond paste slurries from 3.0 to 0.1 µm (Kemet, Maidstone, UK). The Pt working electrodes were polished between experiments using 0.3 µm α-alumina slurry in distilled water. The electrodes were briefly sonicated in distilled water and rinsed with ethanol (GCE) or distilled water (Pt) between each polishing step, to remove any adhered microparticles. The electrodes were then dried in an oven at 100 °C to remove any residual traces of water. The Pt and GCE electroactive area was calibrated for each experiment using a 5 mM ferrocene solution in CH_3CN solvent containing 0.1 M [*n*Bu_4N][PF_6] as the supporting electrolyte. The electroactive area was accurately determined by construction of a Randles-Sevcik plot from cyclic voltammograms recorded at varying scan rates (50-750 mVs^{-1}).[37] The Ag wire pseudo-reference electrodes were calibrated to the ferrocene/ferrocenium couple in CH_2Cl_2 at the end of each run to allow for any drift in potential, following IUPAC recommendations.[52] All electrochemical measurements were performed at ambient temperatures under an inert N_2 atmosphere in CH_2Cl_2 containing 0.05 M [*n*Bu_4N][$B(C_6F_5)_4$] as the supporting electrolyte. All electrochemical measurements were iR-compensated to within 80 ± 5 % of the solution uncompensated resistance.

Na[$HB(C_6Cl_5)_3$], Na[2–H]. A clear colorless solution of 1.0 M Na[$HBEt_3$] in toluene (0.3 mL, 0.30 mmol) was added to a pale yellow suspension of $B(C_6Cl_5)_3$ (0.15 g, 0.20 mmol) in dry toluene (10 mL). The reaction mixture was heated to 80 °C and left to stir under N_2 overnight; warming resulted in dissolution of the suspension to give a pale yellow solution and a white precipitate formed as the reaction progressed. The reaction mixture was allowed to cool, and the precipitate was left to settle, before it was filtered and triturated with dry toluene (2 × 3 mL). The residue was dried in vacuo to yield Na[**2**–H] (0.14 g, 0.18 mmol) as a white powder in 89 % yield. ^1H NMR (300 MHz, [D_6]DMSO, 25 °C, TMS): δ=4.28 (br. m, 1H; BH). ^{11}B NMR (96.3 MHz, [D_6]DMSO, 25 °C, $BF_3.OEt_2$): δ=−8.42 (br.).

[*n*Bu_4N][$HB(C_6Cl_5)_3$], [*n*Bu_4N][2–H]. A clear colorless solution of *n*Bu_4NCl (0.041 g, 0.15 mmol) in dry CH_2Cl_2 (3 mL) was added to a white suspension of Na[**2**–H] (0.12 g, 0.16 mmol) in dry CH_2Cl_2 (3 mL) at room temperature, with stirring under N_2. This resulted in the formation of a fine flocculent precipitate with the simultaneous breakup of the suspended material. The reaction mixture was left to stir overnight. The precipitate was then allowed to settle before it was filtered; the residue was triturated with dry CH_2Cl_2 (2 × 1.5 mL). The filtrate and extracts were combined and concentrated in vacuo to give [*n*Bu_4N][**2**–H] (0.11 g, 0.11 mmol) as a white powder in 77 % yield. Crystals suitable for X-ray crystallography (colorless needles) were grown by dissolving [*n*Bu_4N][**2**–H] in a minimum quantity of dry CH_2Cl_2, warming to approximately 40 °C, adding an equal quantity of dry light petroleum ether and slow-cooling to room temperature. ^1H NMR (300 MHz, $CDCl_3$, 25 °C, TMS): δ=4.32 (br. m, 1H; BH), 3.12 (m, 8H; CH_2), 1.57 (m, 8H; CH_2), 1.35 (m, 8H; CH_2), 0.94 (t, $^3J(H,H)$=7.1 Hz, 12H; CH_3). ^{11}B NMR (96.3 MHz, $CDCl_3$, 25 °C, $BF_3.OEt_2$): δ=−8.68 (d, $^1J(B,H)$ = 76 Hz). ^{13}C NMR (75.5 MHz, $CDCl_3$, 25 °C, TMS): δ=138.2, 138.0, 130.0, 129.7, 127.8, 59.1, 24.1, 19.9, 13.8.

Acknowledgements

GGW and AEA thank the Royal Society for financial support via University Research Fellowships. EJL thanks the EPSRC for financial support *via* a DTA studentship under grant number EP/J500409/. The research leading to these results has received funding from the European Research Council under the ERC Grant Agreement no. 307061.

Keywords: Cyclic voltammetry • Electrocatalysis • Frustrated Lewis pairs • Fuel cells • H transfer

[1] G. C. Welch, R. R. S. Juan, J. D. Masuda, D. W. Stephan, *Science* **2006**, *314*, 1124–1126.
[2] H. C. Brown, H. I. Schlesinger, S. Z. Cardon, *J. Am. Chem. Soc.* **1942**, *64*, 325–329.
[3] D. W. Stephan, in *Comprehensive Inorganic Chemistry II (Second Edition)* (Ed.: J.R. Poeppelmeier), Elsevier, Amsterdam, **2013**, pp. 1069–1103.
[4] D. W. Stephan, G. Erker, *Angew. Chem. Int. Ed.* **2010**, *49*, 46–76.
[5] D. W. Stephan, *Dalton Trans.* **2009**, 3129.
[6] R. M. Bullock, Ed. , *Catalysis Without Precious Metals*, Wiley, **2010**.
[7] D. Holschumacher, T. Bannenberg, C. G. Hrib, P. G. Jones, M. Tamm, *Angew. Chem. Int. Ed.* **2008**, *47*, 7428–7432.
[8] V. Sumerin, F. Schulz, M. Nieger, M. Leskelä, T. Repo, B. Rieger, *Angew. Chem. Int. Ed.* **2008**, *47*, 6001–6003.
[9] G. C. Welch, D. W. Stephan, *J. Am. Chem. Soc.* **2007**, *129*, 1880–1881.
[10] P. Spies, G. Erker, G. Kehr, K. Bergander, R. Fröhlich, S. Grimme, D. W. Stephan, *Chem. Commun.* **2007**, 5072.
[11] G. Ménard, D. W. Stephan, *Angew. Chem. Int. Ed.* **2012**, *51*, 8272–8275.
[12] T. J. Herrington, A. J. W. Thom, A. J. P. White, A. E. Ashley, *Dalton Trans.* **2012**, *41*, 9019.
[13] E. L. Kolychev, T. Bannenberg, M. Freytag, C. G. Daniliuc, P. G. Jones, M. Tamm, *Chem. Eur. J.* **2012**, *18*, 16938–16946.
[14] S. C. Binding, H. Zaher, F. M. Chadwick, D. O'Hare, *Dalton Trans.* **2012**, *41*, 9061–9066.
[15] Z. Lu, Z. Cheng, Z. Chen, L. Weng, Z. H. Li, H. Wang, *Angew. Chem. Int. Ed.* **2011**, *50*, 12227–12231.
[16] J. M. Farrell, J. A. Hatnean, D. W. Stephan, *J. Am. Chem. Soc.* **2012**, *134*, 15728–15731.
[17] A. L. Travis, S. C. Binding, H. Zaher, T. A. Q. Arnold, J.-C. Buffet, D. O'Hare, *Dalton Trans.* **2013**, *42*, 2431.
[18] G. Erker, *Dalton Trans.* **2011**, *40*, 7475–7483.

[19] A. M. Chapman, M. F. Haddow, D. F. Wass, *J. Am. Chem. Soc.* **2011**, *133*, 18463–18478.
[20] M. T. Whited, *Beilstein J. Org. Chem.* **2012**, *8*, 1554–1563.
[21] P. A. Chase, T. Jurca, D. W. Stephan, *Chem. Commun.* **2008**, 1701.
[22] D. W. Stephan, *Org. Biomol. Chem.* **2012**, *10*, 5740–5746.
[23] D. W. Stephan, S. Greenberg, T. W. Graham, P. Chase, J. J. Hastie, S. J. Geier, J. M. Farrell, C. C. Brown, Z. M. Heiden, G. C. Welch, et al., *Inorg. Chem.* **2011**, *50*, 12338–12348.
[24] S. D. Tran, T. A. Tronic, W. Kaminsky, D. Michael Heinekey, J. M. Mayer, *Inorg. Chim. Acta* **2011**, *369*, 126–132.
[25] A. E. Ashley, A. L. Thompson, D. O'Hare, *Angew. Chem. Int. Ed.* **2009**, *48*, 9839–9843.
[26] C. M. Mömming, E. Otten, G. Kehr, R. Fröhlich, S. Grimme, D. W. Stephan, G. Erker, *Angew. Chem. Int. Ed.* **2009**, *48*, 6643–6646.
[27] E. J. Lawrence, V. S. Oganesyan, D. L. Hughes, A. E. Ashley, G. G. Wildgoose, *J. Am. Chem. Soc.* **2014**, *136*, 6031–6036.
[28] E. J. Lawrence, T. J. Herrington, A. E. Ashley, G. G. Wildgoose, *Angew. Chem. Int. Ed.* **2014**, *53*, 9922–9925.
[29] C. P. de Leon, F. C. Walsh, D. Pletcher, D. J. Browning, J. B. Lakeman, *J. Power Sources* **2006**, *155*, 172–181.
[30] B. H. Liu, Z. P. Li, *J. Power Sources* **2009**, *187*, 291–297.
[31] J. Ma, N. A. Choudhury, Y. Sahai, *Renew. Sust. Energ. Rev.* **2010**, *14*, 183–199.
[32] D. M. F. Santos, C. A. C. Sequeira, *Renew. Sust. Energ. Rev.* **2011**, *15*, 3980–4001.
[33] I. Merino-Jiménez, C. Ponce de León, A. A. Shah, F. C. Walsh, *J. Power Sources* **2012**, *219*, 339–357.
[34] E. J. Lawrence, T. J. Herrington, A. E. Ashley, G. G. Wildgoose, *Angew. Chem. Int. Ed.* **2014**, DOI 10.1002/anie.201405721R1.
[35] A. E. Ashley, T. J. Herrington, G. G. Wildgoose, H. Zaher, A. L. Thompson, N. H. Rees, T. Krämer, D. O'Hare, *J. Am. Chem. Soc.* **2011**, *133*, 14727–14740.
[36] E. J. Lawrence, V. S. Oganesyan, G. G. Wildgoose, A. E. Ashley, *Dalton Trans.* **2013**, *42*, 782–789.
[37] R. G. Compton, C. E. Banks, *Understanding Voltammetry*, Imperial College Press, London, **2011**.
[38] T. Iwasita, *Electrochim. Acta* **2002**, *47*, 3663–3674.
[39] M. J. Croissant, T. Napporn, J.-M. Léger, C. Lamy, *Electrochim. Acta* **1998**, *43*, 2447–2457.
[40] T. Zhang, A. B. Anderson, *J. Phys. Chem. C* **2007**, *111*, 8644–8648.
[41] P. Jutzi, C. Müller, A. Stammler, H.-G. Stammler, *Organometallics* **2000**, *19*, 1442–1444.
[42] D. Griller, K. U. Ingold, *Acc. Chem. Res.* **1980**, *13*, 317–323.
[43] C. Chatgilialoglu, K. U. Ingold, J. C. Scaiano, *J. Am. Chem. Soc.* **1981**, *103*, 7739–7742.
[44] S. U. Pedersen, T. Lund, *Acta. Chem. Scand.* **1991**, *45*, 397–402.
[45] P. Cauliez, M. Benaskar, A. Ghanimi, J. Simonet, *New J. Chem.* **1998**, *22*, 253–261.
[46] E. Duñach, A. P. Esteves, A. M. Freitas, M. J. Medeiros, S. Olivero, *Tetrahedron Lett.* **1999**, *40*, 8693–8696.
[47] D. M. Fang, D. G. Peters, M. S. Mubarak, *J. Electrochem. Soc.* **2001**, *148*, E464–E467.
[48] A. P. Esteves, A. M. Freitas, M. J. Medeiros, D. Pletcher, *J. Electroanal. Chem.* **2001**, *499*, 95–102.
[49] S. J. Lancaster, *ChemSpider SyntheticPages* **2003**, DOI: 10.1039/SP215.
[50] R. J. LeSuer, C. Buttolph, W. E. Geiger, *Anal. Chem.* **2004**, *76*, 6395–6401.
[51] R. C. Srivastava, *J. Chem. Res. (S)* **1985**, 330–331.
[52] G. Gritzner, J. Kůta, *Electrochim. Acta* **1984**, *29*, 869–873.

Entry for the Table of Contents (Please choose one layout)

Layout 1:

FULL PAPER

Platinum is a non-innocent catalytic electrode material for the electrochemical-frustrated Lewis pair system based on $B(C_6F_5)_3$. The mechanism of $[HB(C_6F_5)_3]^-$ oxidation at a platinum electrode is dominated by hydrogen atom transfer (HAT). The operation of this mechanism gives rise to a strong electrocatalytic effect – a 390 mV reduction in the required oxidation potential and an increase in measured current density.

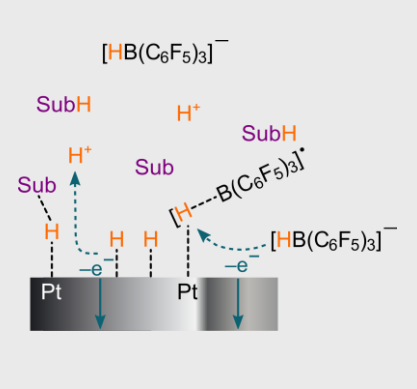

*Elliot J. Lawrence, Robin J. Blagg, David L. Hughes, Andrew E. Ashley, Gregory G. Wildgoose**

Page No. – Page No.

A combined "electrochemical-frustrated Lewis pair" approach to hydrogen activation: surface catalytic effects at platinum electrodes